The linear threshold of the ion-temperature-gradient-driven mode

Cite as: Physics of Fluids B: Plasma Physics **5**, 520 (1993); https://doi.org/10.1063/1.860537
Submitted: 20 April 1992 . Accepted: 11 September 1992 . Published Online: 01 September 1998

S. C. Guo, and F. Romanelli

The linear threshold of the ion-temperature-gradient-driven mode

S. C. Guo[a] and F. Romanelli
Associazione EURATOM–ENEA sulla Fusione, Centro Ricerche Energia, 00044, Frascati, Roma, Italy

(Received 20 April 1992; accepted 11 September 1992)

A comprehensive stability analysis of the ion-temperature-gradient-driven mode in various parameter domains is presented. The effect of parallel ion dynamics on the threshold value in toroidal geometry is investigated for the short-wavelength and finite-shear limits. A general explicit expression for the threshold is given, which is in agreement with the results obtained by solving the full integrodifferential equation. The destabilizing effect of trapped electrons below the threshold is qualitatively similar to the results of local theory, but electron collisionality has to be sufficiently weak. In the long-wavelength limit, two branches exist, respectively, toroidal and slablike in character. The toroidal branch has been investigated elsewhere [Romanelli *et al.*, Phys. Fluids B **3**, 2496 (1991)]. In this paper, the stability of the slablike branch is studied both analytically and numerically. The trapped-ion effects on the threshold are discussed in detail.

I. INTRODUCTION

The anomalous transport observed in tokamak plasmas is associated with the presence of small-scale turbulence.[1] Among the various instabilities, many experimental results are in favor of the ion-temperature-gradient-driven mode (η_i mode $\eta_i = d \ln T_i / d \ln n$) as a major candidate for explaining anomalous transport. The η_i mode is, indeed, a robust, fluidlike instability, and it is very likely that such a mode could play a role in affecting the energy transport. Moreover, the improvement in confinement observed in the presence of peaked density profiles and in the hot ion mode regime of operation is in agreement with the relevant features of the η_i-mode stability analysis.[1] However, in order to precisely quantify the role of the η_i mode, detailed knowledge of the stability threshold is required. This is not a trivial task because many physical effects can be important near the threshold. In fact, the stability analysis of the η_i mode has often been carried out by making very crude approximations in order to allow a simple solution to the problem. This has provided a qualitative understanding of many different features of the η_i-mode dynamics, but has not solved the problem of precise determination of the η_i-mode threshold in the different parameter regimes of interest for a tokamak plasma.

The aim of the present paper is to provide a unified picture of η_i-mode dynamics by clarifying the limits of the various stability analyses and by providing expressions for the threshold that are valid in all the parameter ranges of interest for a tokamak. In order to accomplish this task, the stability analysis is discussed for both short and long wavelengths and the results are systematically compared with the results of previous stability analyses. For the sake of simplicity, only the case of a pure plasma with circular shape and low β is considered and the electrostatic approximation is employed. Nevertheless, the range of validity of our results covers all of the collisionality domain of interest, long and short wavelengths, moderately low and finite shear, and peaked and flat density profiles. In addition, we fully account for the effects related to toroidal geometry, as in standard neoclassical theory.

The η_i instability was first discovered by Rudakov and Sagdeev[2] within the context of a local fluid analysis and later discussed for a sheared slab by Coppi *et al.*[3] The slab model equilibrium has been employed by several authors: in particular, Antonsen *et al.*;[4] Hassam *et al.*[5] have discussed the fluid limit, while Hahm and Tang[6] have studied the fully kinetic limit. However, as shown by Coppi and Pegoraro[7] and by Horton *et al.*,[8] in a toroidal system the instability is mainly driven by the effect of the magnetic field curvature. Unfortunately, a complete kinetic analysis of toroidal equilibria involves the solution of a Fredholm integral equation of the second kind.[9–12] Therefore, in order to simplify the analysis, most of the papers have considered only particular limits of the general equations in toroidal geometry. Fluid models have been considered in Ref. 13 and by Guzdar *et al.*,[14] Jarmen *et al.*,[15] Shukla,[16] and by Dominguez and Waltz.[17] References 14–17 have attempted to give a precise determination of the linear threshold by retaining terms in the fluid expansion higher than the lowest-order term, but they have the fundamental problem that, near threshold, the fluid approximation cannot be applied since the mode is affected by both magnetic drift and Landau resonance. Other papers have incorporated the effect of ω_{di} resonance while neglecting Landau resonance. Implicit in these analyses is the assumption that the effect of parallel dynamics is only to localize the eigenfunction in the bad curvature region, while the effect on the threshold is negligible. This allows the ω_{di} term to be replaced by the value at the outside of the torus. Such an approximation has been employed by Terry *et al.*[18] for the case of peaked density profiles and in Ref. 19 for the case of flat density profiles. A nonlocal analysis based on the same assumption has been performed by Cheng and Tsang,[20] who have also retained the first-order correction associated to parallel dynamics, and in Ref. 21, where the

[a]Permanent address: Institute of Physics, Chinese Academy of Sciences, P.O. Box 603, 100080, Beijing, People's Republic of China.

 0899-8221/93/020520-14$06.00

effect of Landau resonance has been considered but with the first-order correction associated to magnetic curvature retained perturbatively. The effect of parallel dynamics has been discussed by Dominguez and Rosenbluth[22] within the context of a local analysis that retains both ω_{di} and Landau resonance. Finally, the effect of nonadiabatic trapped-electron dynamics has been considered in Refs. 23 and 24, where it has been shown that the mode can always be unstable for peaked density profiles. Previous papers have considered the case of moderate shear and short wavelengths ($k_\theta \rho_i \lesssim 1$). In this regime, the mode has a moderate ballooning structure and can be destabilized by a combination of parallel dynamics and curvature. More recently, the long-wavelength, low-shear regime has received more attention. It has been recently pointed out in Ref. 25 that at long wavelengths two branches can be unstable, a toroidal and a slablike branch. The eigenfunctions belonging to the former branch are characterized by a dominant variation over the connection length scale and are stabilized by the ion transit resonance.[26] The slablike branch is characterized by eigenfunctions varying mainly over the secular scale with small superimposed oscillations over the connection length scale. The latter can produce a resonance between the mode frequency and the ion transit frequency, as in the case of the toroidal branch. However, as shown in Ref. 26, such a resonance does not significantly affect the threshold condition. In addition, the mode frequency tends to be smaller than the ion transit frequency, and the trapped-ion dynamics can be expected to strongly affect the mode dynamics. This effect, which has also been investigated by Biglari *et al.*[27] and by Xu and Rosenbluth[28] using a simple dispersion relation that neglects the effect of circulating ions, is fully discussed in the present paper. In this limit, it is shown that the radial drift of circulating ions significantly enhances the mode threshold, while trapped ions drive an interchangelike mode similar to the conventional trapped-ion mode. Finite-β corrections,[29] nonisotropy effects,[30] impurities,[31] and neoclassical collisional effects[32] are neglected.

The paper is set out as follows. In Sec. II the general formalism is presented. In Sec. III we discuss the short-wavelength limit. In Sec. IV the long-wavelength threshold for the toroidal branch is considered, while the long-wavelength threshold for the slab branch is discussed in Sec. V. The conclusions are given in Sec. VI.

II. GENERAL FORMALISM

The electron response and the ion response are obtained by solving the gyrokinetic equation,[33]

$$\frac{v_\parallel}{qR}\frac{\partial}{\partial\theta}H_j - i(\omega-\omega_{Dj})H_j = -i\frac{e_jF_{Mj}}{T_j}(\omega-\omega_{*Tj})\phi J_0(\alpha), \tag{1}$$

where q is the safety factor, R is the major radius, H_j is the nonadiabatic part of the distribution function, $f_j = -e\phi F_{Mj}/T_j + H_j J_0(\alpha_j)$, ϕ is the electrostatic potential, J_0 is a Bessel function of argument $\alpha_j = k_\perp \rho_j v_\perp$,

$$\omega_{*Tj} = \omega_{*j}[1+\eta_j(E-3/2)],$$

$$\omega_{Dj} = \omega_{D0j}(\cos\theta + s\theta\sin\theta),$$

$$\omega_{D0j} = -2ck_\theta T_j/(e_jBR)(v_\perp^2/2 + v_\parallel^2),$$

$$\omega_{*j} = -ck_\theta T_j/(e_jBL_{nj}),$$

$$L_{nj} = -n_0/\nabla n_{0j}, \quad \eta_j = d\ln T_j/d\ln n,$$

B is the equilibrium magnetic field, the velocity is normalized to the thermal velocity $v_{tj} = (2T_j/m_j)^{1/2}$, $E = v^2$ is the energy, $\rho_j = v_{tj}/\Omega_j$, and the index j labels the species. As usual, we employ the ballooning representation[34] and consider a low-β equilibrium with circular magnetic surfaces, so $B = B_0/(1+\epsilon\cos\theta)$, where $\epsilon = r/R$ is the inverse aspect ratio.

The trapped-electron response is obtained by expanding Eq. (1) in ω/ω_{be}, where ω_{be} is the electron bounce frequency, yielding[35,36]

$$\frac{n_{eT}}{n_0} = (2\epsilon)^{1/2}\frac{e\phi(\theta)}{T_e} + \delta_T(\omega)\int_0^1 \frac{d\kappa^2}{8K(\kappa)} \times \sum_{p=-\infty}^{+\infty} g(\kappa,\theta-2\pi p)\int_{-\infty}^{+\infty} d\theta'\, g(\kappa,\theta') \times \frac{e\phi(2\pi p-\theta')}{T_e}, \tag{2}$$

with

$$\delta_T(\omega) = -\frac{2}{\sqrt{\pi}}(2\epsilon)^{1/2}\int_0^\infty dE\, E^{1/2} \times \frac{\omega-\omega_{*Te}}{\omega-\overline{\omega_{De}}+i\nu_{e\,\mathrm{eff}}E^{-3/2}}e^{-E}, \tag{3}$$

where $\overline{\omega_{De}}$ is the bounce-averaged electron magnetic drift frequency, K is a complete elliptic integral of the first kind, and

$$g(\kappa,\theta) = \int_{-\theta_0}^{+\theta_0}\frac{d\theta'\,\delta(\theta-\theta')}{(\kappa^2-\sin^2\theta'/2)^{1/2}}. \tag{4}$$

In the above expressions, $\kappa = \sin(\theta_0/2) = [1-\mu B_0(1-\epsilon)/E]/\epsilon$, $\mu = v_\perp^2/B$ is the magnetic moment and $\nu_{e\,\mathrm{eff}} = \nu_{ei}/\epsilon$, with ν_{ei} the electron–ion collision frequency. In deriving Eq. (3), the usual Krook collision operator has been used.[36]

Finally, upon assuming adiabatic response for the circulating electrons, the quasineutrality equation can be written as

$$[1-(2\epsilon)^{1/2}]\frac{e\phi}{T_e} + \frac{n_{eT}}{n_0} = -\frac{e\phi}{T_i} + \int d^3v\, H_j J_0(\alpha). \tag{5}$$

In order to determine an explicit expression for H_j, an ordering scheme appropriate to the short- and long-wavelength limits has to be defined. To this aim, it is convenient to start with the fluid limit of the quasineutrality equation for the η_i mode,[8,19]

$$\frac{\omega_{ti}^2}{2\omega^2}\frac{\partial^2\phi}{\partial\theta^2}+\left(\frac{(1+\delta_T)/\tau+\omega_{*i}/\omega}{1-\omega_{*pi}/\omega}\right.$$

$$\left.+(k_\theta\rho_i)^2(1+s^2\theta^2)+\frac{\omega_D}{\omega}\right)\phi=0 \tag{6}$$

with $\omega_D=2ck_\theta T_i/(eBR)(\cos\theta+s\theta\sin\theta)$, $\tau=T_e/T_i$, and $\omega_{*pi}=\omega_{*i}(1+\eta_i)$, $\omega_{ti}=v_{ti}/Rq$. The standard short-wavelength ordering corresponds to balancing parallel ion compressibility, curvature, inertia, and adiabatic electron response on the connection length scale $\theta\approx1$, yielding[8,19] $|\omega|\approx|\omega_{*pi}\omega_D|^{1/2}$, $k_\theta\rho_i\approx\epsilon_T^{1/4}$, and $\theta\approx1$. In this limit, the eigenfunction has a moderate ballooning structure which can be analytically determined within the strong coupling approximation,[37] yielding $\phi\approx\exp(i\sigma\theta^2)$ with $\omega\approx(\omega_{*pi}\omega_D)^{1/2}(2+is/q)^{1/2}$ and $\sigma\approx[(k_\theta\rho_i)^2Rsq\omega/(2L_T\omega_{*i})]$. We assume that in the kinetic analysis the eigenfunction remains localized in the ballooning space in such a way that the strong coupling approximation can be applied, but we fully account for the effect of parallel dynamics. In this case, after replacing the magnetic drift resonance with the value at $\theta=0$, Eq. (1) can be conveniently solved in the Fourier transformed space (i.e., in real space), rather than in the ballooning space, by defining $H(\theta)=\int dz\, e^{iz\theta}\hat{H}(z)$ and $\phi(\theta)=\int dz\, e^{iz\theta}\hat{\phi}(z)$. Upon making the small Larmor radii assumption, it is possible to expand the Bessel function J_0 in Eqs. (1) and (5) for small arguments. Thus, the solution of Eq. (1) in the Fourier transformed space can be written as

$$\hat{H}(z)=\frac{\omega-\omega_{*Ti}}{\omega-\omega_{D0i}-(v_\parallel/qR)z}\times F_{Mi}\left\{1-\frac{b_i v_\perp^2}{4}\left[1-\left(s\frac{d}{dz}\right)^2\right]\right\}\frac{e\hat{\phi}}{T_i}.$$

Inserting in Eq. (5) and dropping the hat, after some algebra, the following differential equation is obtained:

$$\frac{b_s}{\tau}s^2\frac{d}{dz}B(z)\frac{d\phi}{dz}-\left(1+\frac{1+\delta_T}{\tau}-A(z)+\frac{b_s}{\tau}B(z)\right.$$

$$\left.-\frac{b_s}{2\tau}s^2\frac{d^2}{dz^2}B(z)\right)\phi=0 \tag{7}$$

with

$$A(z)=\int d^3v\, F_M\frac{\omega-\omega_{*Ti}}{\omega-\omega_{D0i}-(v_\parallel/qR)z} \tag{8}$$

and

$$B(z)=\int d^3v\, F_M v_\perp^2\frac{\omega-\omega_{*Ti}}{\omega-\omega_{D0i}-(v_\parallel/qR)z}. \tag{9}$$

In Eqs. (7)–(9), the variable z is the Fourier conjugate of the variable θ and is related to the radial distance from the mode rational surface r_s by $z=nq'(r-r_s)$, with n the toroidal number. The term proportional to $B(z)$ is the finite Larmor radius correction. After solving Eq. (7), the localization condition of the eigenfunction has to be checked *a posteriori*. In particular, the strong coupling approximation requires the width of the eigenfunction Δz to be larger than the distance between mode rational surfaces, which corresponds to $\Delta z=1$. A discussion of Eq. (7) is presented in the next section.

In the long-wavelength limit ($k_\theta\rho_i\ll\epsilon_T^{1/4}$), the eigenfunction becomes broad and the strong coupling approximation can no longer be applied. In this case, two branches exist, a toroidal and a slablike branch.[25] The eigenmode considered in this paper in the short-wavelength limit is connected with the toroidal branch in the long-wavelength limit. The eigenfunctions belonging to such a branch exhibit a fast variation, along the equilibrium field, over the connection length scale with an envelope varying over a secular scale. The other branch, which also exists in slab geometry, is characterized by a variation along the equilibrium magnetic field dominated by the secular scale, with small superimposed oscillations over the connection length scale. It is convenient to define two different ordering schemes for the toroidal and the slab eigenmodes, respectively. The toroidal ordering, as given in Ref. 26, is obtained by balancing parallel compressibility and adiabatic electron response on the scale $\theta\approx1$, yielding $\omega\approx(\omega_{*pi}\omega_{ti}^2)^{1/3}$. The width of the envelope along the equilibrium magnetic field is obtained by balancing parallel compressibility and geodesic curvature on the secular scale, yielding $\theta\approx[\epsilon_T^{1/2}/(k_\theta\rho_i)^2]^{1/3}$. The effect of parallel compressibility becomes important for $\omega\approx\omega_{ti}$ corresponding to $k_\theta\rho_i\approx\epsilon_T$. Therefore, the optimum ordering for the toroidal branch is given by $\omega\approx\omega_{*pi}\approx\omega_{ti}$, $k_\theta\rho_i\approx\epsilon_T$ and $\theta\approx\epsilon_T^{-1/2}$. Note that, within such an ordering, the trapped-electron response is smaller than the ion response by a factor $\epsilon^{1/2}$ and it provides only minor modifications to the dynamics of the mode. The toroidal branch dispersion relation from Ref. 26 is

$$1+\frac{1}{\tau}(1+\delta_T)+\Omega^2\left\{\frac{2\lambda}{\Omega}+\left[1+\frac{2\lambda}{\Omega}\left(\Omega^2-\frac{1}{2}+\frac{1}{\eta_i}\right)\right]\right.$$

$$\left.\times\frac{1}{\Omega}Z(\Omega)\right\}=0, \tag{10}$$

where Z is the plasma dispersion function, $\Omega=2\omega/\omega_{ti}$, and $\lambda=qk_\theta\rho_i/2^{1/2}\epsilon_T$.

For the slablike branch, the effect associated with the ion transit resonance has been studied in Ref. 26. However, near the threshold, the frequency tends to be smaller than ω_{ti} and the trapped-ion effect has to be considered. Therefore, we assume a different approach here and obtain the slab ordering by balancing inertia, parallel compressibility, and adiabatic electron response on the secular scale rather than on the connection length scale. Upon introducing $\delta=k_\theta\rho_i$ as a smallness parameter, but ordering $\epsilon_T=O(1)$, the following ordering is obtained: $\omega\approx(\omega_{*pi}k_\theta\rho_i\omega_{ti})^{1/2}\approx\delta\omega_{ti}$ and $\theta\approx[\epsilon_T^{1/2}/(k_\theta\rho_i)^2]^{1/2}\approx\delta^{-1}$. In this case, the effect of parallel compressibility is important on the secular scale, and the stability of the mode is determined by the Landau resonance $\omega\approx k_\parallel v_{ti}$. Using this ordering, it is possible to derive the quasineutrality equation as shown in Appendix A, yielding an equation formally similar to Eq. (7), that is

$$\frac{d^2\psi}{dz^2}+\frac{1}{4}\frac{(dB_2/dz)^2}{B_2^2}\psi-\frac{1}{b_s s^2 B_2}(1+\tau+\delta_T-A\tau+b_s B_1)\psi$$

$$=0. \tag{11}$$

Here, $\psi=\phi/\sqrt{B_2}$, $A=A^{(c)}+A^{(t)}$, $B_j=B_j^{(c)}+B_j^{(t)}$, $j=1,2$, and

$$A^{(c)}=\frac{\omega_{ti}}{2\sqrt{\pi}}\sum_\sigma\int_c\frac{B_0\,d\mu\,dE}{\omega_s}F_M\frac{\omega-\omega_{*T}}{\omega-\langle\omega_{Db}\rangle_c-\omega_s z}, \tag{12}$$

$$B_1^{(c)}=\frac{\omega_{ti}}{2\sqrt{\pi}}\sum_\sigma\int_c\frac{B_0\,d\mu\,dE}{\omega_s}F_M\mu B_0\frac{\omega-\omega_{*T}}{\omega-\langle\omega_{Db}\rangle_c-\omega_s z}, \tag{13}$$

$$B_2^{(c)}=\frac{\omega_{ti}}{2\sqrt{\pi}}\sum_\sigma\int_c\frac{B_0\,d\mu\,dE}{\omega_s}F_M\left(\mu B_0+2q^2\frac{\langle\alpha^2\rangle_c}{\epsilon}\right)\times\frac{\omega-\omega_{*T}}{\omega-\langle\omega_{Db}\rangle_c-\omega_s z}, \tag{14}$$

$$A^{(t)}=\frac{\omega_{ti}}{2\sqrt{\pi}}\sum_\sigma\int_c\frac{B_0\,d\mu\,dE}{\omega_b}F_M\times\frac{\omega-\omega_{*T}}{\omega-\langle\omega_{Db}\rangle_t-(s/\epsilon)\omega_{D0}\langle\alpha v_\parallel\rangle_t+iv_{i\,\mathrm{eff}}/E^{3/2}}, \tag{15}$$

$$B_1^{(t)}=\frac{\omega_{ti}}{2\sqrt{\pi}}\sum_\sigma\int_c\frac{B_0\,d\mu\,dE}{\omega_b}F_M\mu B_0\times\frac{\omega-\omega_{*T}}{\omega-\langle\omega_{Db}\rangle_t-(s/\epsilon)\omega_{D0}\langle\alpha v_\parallel\rangle_t+iv_{i\,\mathrm{eff}\,i}/E^{3/2}}, \tag{16}$$

$$B_2^{(t)}=\frac{\omega_{ti}}{2\sqrt{\pi}}\sum_\sigma\int_c\frac{B_0\,d\mu\,dE}{\omega_b}F_M\left(\mu B_0+2q^2\frac{\langle\alpha^2\rangle_c}{\epsilon}\right)\times\frac{\omega-\omega_{*T}}{\omega-\langle\omega_{Db}\rangle_t-(s/\epsilon)\omega_{D0}\langle\alpha v_\parallel\rangle_t+iv_{i\,\mathrm{eff}\,i}/E^{3/2}}, \tag{17}$$

where α, ω_s, and ω_b are defined in Appendix A. Note that, while $B_1^{(t)}$ and $B_1^{(c)}$ are associated with the conventional finite Larmor radius corrections, the terms $B_2^{(t)}$ and $B_2^{(c)}$ account for drift orbit corrections and tend to dominate over $B_1^{(t)}$ and $B_1^{(c)}$, The superscripts (c) and (t) represent circulating and trapped particle contribution, respectively.

III. SHORT-WAVELENGTH TOROIDAL BRANCH

It is apparent from the expression of the growth rate in the fluid approximation[19] $[\omega\approx(\omega_{*pi}\omega_D)^{1/2}(2+is/q)^{1/2}]$ that the effect of parallel dynamics is subdominant with respect to the effect of curvature for $s/q\ll 2$. Meanwhile, the localization of the mode depends on the balance between parallel dynamics and inertia. As a working hypothesis, we can assume that in a kinetic analysis the dominant effect on the growth rate is the effect associated to ω_D, with parallel dynamics simply providing the localization of the eigenfunction in such a way that the ω_D term can be replaced with its value at $\theta=0$. Neglecting the finite ion Larmor radius term in Eq. (7) and the $k_\parallel v_\parallel$ term in the denominator of the nonadiabatic circulating ion response, the following dispersion relation is obtained:

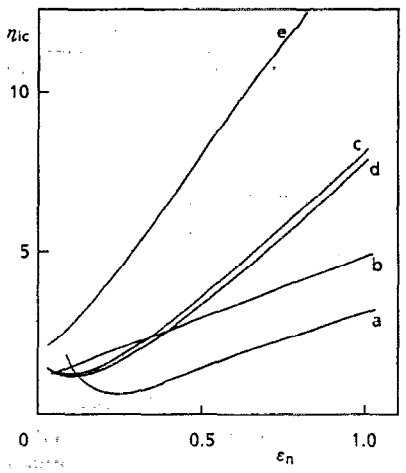

FIG. 1. The threshold value η_{ic} vs ϵ_n in the short-wavelength limit. Curve a is the result from the local analysis Eq. (18). Curve b is obtained by solving Eq. (20), corresponding to the sheared slab limit. Curve c is obtained from Eq. (7) which takes into account parallel dynamics and curvature effects in the circulating ion responses for $b_s=0.1$ and $s=q=\tau=1$. Curve d is also obtained from Eq. (7), but for $s=q=2$ and $\tau=1$. Curve e corresponds to the long-wavelength toroidal branch for $b_s=0.01$ and $q=\tau=1$.

$$1+\frac{1}{\tau}-\int d^3v\,F_M\frac{\omega-\omega_{*T}}{\omega-\omega_{D0i}}=0. \tag{18}$$

Equation (18) has been studied in Refs. 18 and 19, and in Ref. 23 by also accounting for the trapped-electron dynamics. In the flat density limit, Eq. (18) yields the following threshold value:

$$\eta_{ic}=\frac{4}{3}\left(1+\frac{1}{\tau}\right)\epsilon_n. \tag{19}$$

The threshold obtained by Eq. (18) is shown in the η_i vs ϵ_n plane in Fig. 1 (curve a) for $\tau=1$. This result is rigorously valid for finite values of shear and $q\to\infty$. For small ϵ_n values, Eq. (18) yields a minimum value of the threshold around $\eta_i=2/3$. A numerical study of the exact integro-differential equation describing the stability of the mode[19] has shown that the assumption of negligible parallel dynamics is, indeed, reasonable for $s/q\leqslant 0.3$.

For s/q values much larger than unity, the effect of parallel dynamics becomes dominant. Neglecting the effect of curvature in the circulating ion response, Eqs. (8) and (9), the sheared slab limit is recovered,[6,21]

$$\frac{d^2}{dz^2}\phi+\left(-b_i+\frac{1+1/\tau+(1-\omega_{*i}/\omega+\eta_i\omega_{*i}/2\omega)Z_i\xi_i-(\eta_i\omega_{*i}/\omega)\xi_i^2(1+Z_i\xi_i)}{(1-\omega_{*i}/\omega-\eta_i\omega_{*i}/2\omega)Z_i\xi_i-(\eta_i\omega_{*i}/\omega)\xi_i^2(1+Z_i\xi_i)}\right)\phi=0, \tag{20}$$

with $\xi_i=\omega/k_\parallel v_{ti}$. The numerical solution of Eq. (20) has shown that the η_i threshold can be fitted by

$$\eta_{ic}=\eta_{i0}(b_s)+\alpha_s(b_s)\left(1+\frac{1}{\tau}\right)\frac{s}{q}\epsilon_n. \tag{21}$$

The dependence of η_{i0} and α_s on b_s is shown in Fig. 2. In Fig. 1, η_{ic} obtained by numerically solving Eq. (20) is shown for $\tau=1$, $s=1$, and $q=1$ (curve b). This result is in good agreement with the analytic estimate given in Ref. 6. On comparing Eqs. (19) and (21) it is easily seen that, while the two expressions give similar estimates for typical values of the parameters, the dependence on s and q is different. Indeed, Eq. (19) has no dependence on s and q because parallel dynamics has been neglected in the analysis. In this case, the threshold is determined by the resonance with the ion magnetic drift frequency, which accounts for the dependence of η_{ic} on toroidicity through the factor ϵ_n. Meanwhile, Eq. (21) has an explicit s/q dependence associated with the effect of ion Landau damping, but when this effect is turned off, e.g., by taking the limit $q\to\infty$, the threshold has no residual dependence on toroidicity because the magnetic drift resonance has been neglected.

In this paper the mode threshold is determined by solving Eq. (7), in which the parallel ion dynamics, the magnetic drift resonance, and the finite Larmor radius corrections are all taken into account. It is convenient to neglect at first the effect of trapped electrons. The marginal stability curve is shown in Fig. 1 in the η_i vs ϵ_n plane for $\tau=1$, $s=1$, and $q=1$ (curve c). The growth rate of the mode versus η_i is shown in Fig. 3. For $\epsilon_n\to 0$, the threshold approaches an almost constant value $\eta_{ic}\approx 1.2$, while in the flat density limit, a convenient representation for the threshold is

$$\eta_{ic}=\frac{4}{3}\left(1+\frac{1}{\tau}\right)\left(1+\alpha_T\frac{s}{q}\right)\epsilon_n, \tag{22}$$

with $\alpha_T\approx 2$. Curve d shows the threshold value η_{ic} vs ϵ_n for $s=q=2$ and $\tau=1$. It is apparent that curves c and d are almost coincident, since the value of s/q is the same for both curves ($s/q=1$). For $q\to\infty$, Eq. (22) can readily recover the result from local theory given by Eq. (19); it is also qualitatively similar to the result of Hahm and Tang[6] for the sheared slab limit ($s/q\gg 1$). Moreover, the η_{ic} value given in Eq. (22) is in agreement, within 10%, with the value obtained from the full numerical solution presented in Ref. 19 [$\eta_{ic}\approx 4$ for $\tau=1$, $s=0.5$, and $q=1.5$ instead of $\eta_{ic}\approx 4.4$ from Eq. (22)]. The result is also in agreement with a more recent analysis of the full equation.[12,28] To be specific, in Ref. 12 from the numerical analysis of the integral equation the parameter $\epsilon_{Tc}=\epsilon_n/\eta_{ic}$ was found to be $\epsilon_{Tc}=0.2$ for $\tau=1$, $s=0.5$, and $q=1.5$, while Eq. (22) predicts $\epsilon_{Tc}=0.225$; in Ref. 28, on the basis of linearized gyrokinetic particle simulations, a threshold value $\epsilon_{Tc}=0.21$ was found for $\tau=1$, $s=1$, and $q=2$, while Eq. (22) predicts $\epsilon_{Tc}=0.19$. In Table I the values of ϵ_{Tc} from the various theories are compared. It is important to recall that the range of validity of Eq. (22) corresponds to moderate values of shear, arbitrary values of q, and wavelengths in the range $b_i\approx\epsilon_T^{1/2}$.

We now consider the effect of trapped-electron dynamics on the mode stability. As discussed in Ref. 23, we can expect very little effect in the flat density limit because the strongly stabilizing mechanism associated with the ion resonances cannot be overcome by the destabilizing effect of the trapped-electron dynamics. This is shown in Fig. 4 for $\epsilon=0.15$. For low ϵ_n values, the mode propagates in the electron diamagnetic direction and is not affected by the ion magnetic drift resonance. However, ion Landau resonance still provides a strong stabilizing mechanism and, unless the trapped-electron response is large, we can expect the mode to be stable. The presence of Landau resonance

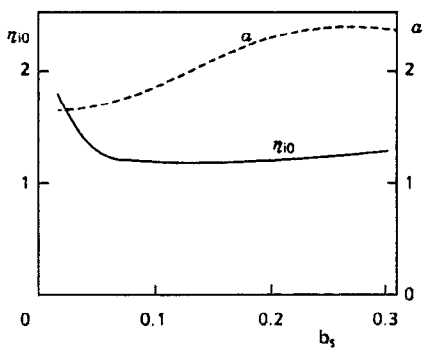

FIG. 2. The dependence of the parameters η_{i0} and α_s of Eq. (21) on b_s.

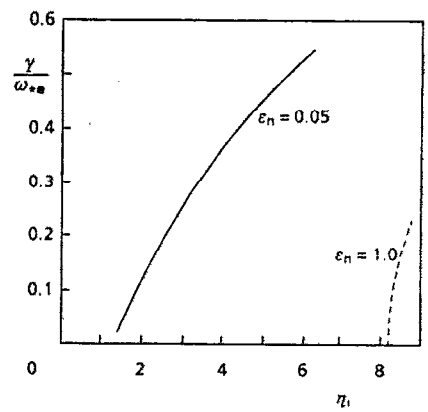

FIG. 3. The growth rates as a function of η_i for different ϵ_n values and $b_s=0.1$, $s=q=\tau=1$ in the short-wavelength limit.

TABLE I. The flat density threshold according to various analyses, for $\tau=1$. The shear and safety factor values are $s=0.5$, $q=1.5$ in the case of Refs. 12, 19, $s=q=1$ in the case of Ref. 6, and $s=1$, $q=2$ in the case of Ref. 28.

	ϵ_{Tc}	ϵ_{Tc} from Eq. (22)
Local kinetic[19]	0.37	0.225
Slab[6]	0.27	0.125
Full kinetic[19]	0.25	0.225
Full kinetic[12]	0.20	0.225
Full kinetic[28]	0.21	0.187

can produce some difference with respect to Ref. 23, in which, since the mode propagates in the electron diamagnetic direction, no stabilizing ion effects are present and an arbitrary small nonadiabatic trapped-electron term can destabilize the mode. From Fig. 4 it can be seen that the mode can be unstable below $\eta_{ic}\simeq 1.2$, for sufficiently low electron collisionality. In this case, the stability boundaries are similar to those obtained in Ref. 23, where the effect of ion Landau damping was neglected. For high values of collisionality, the trapped-electron response is small and the mode is strongly stable. The real and imaginary parts of the eigenvalue are shown in Fig. 5 as a function of η_i and three collisionality values. The transition from the unstable to the stable situation for $\eta_{ic}<1.2$ is quite sharp and it is possible to define a critical value for the collisionality parameter $\nu_{ec}=\nu_{e\,\mathrm{eff}}/\omega_{*e}$, at which the region below $\eta_i=1.2$ becomes stable. In Fig. 6 such a critical value is shown as a function of s/q. For $q\to\infty$, the mode is unstable also for large collisionality values, in agreement with the results of

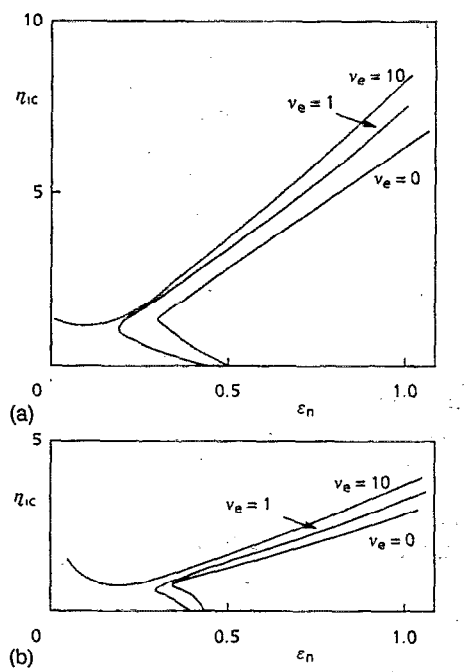

FIG. 4. Plot of η_{ic} vs ϵ_n for different values of the trapped-electron effective collisionality, $\nu_e=|\nu_{e\,\mathrm{eff}}/\omega_{*e}|$, $b_s=0.1$, $\epsilon=0.15$, $s=\tau=1$, and (a) $q=1$; (b) $q=5$.

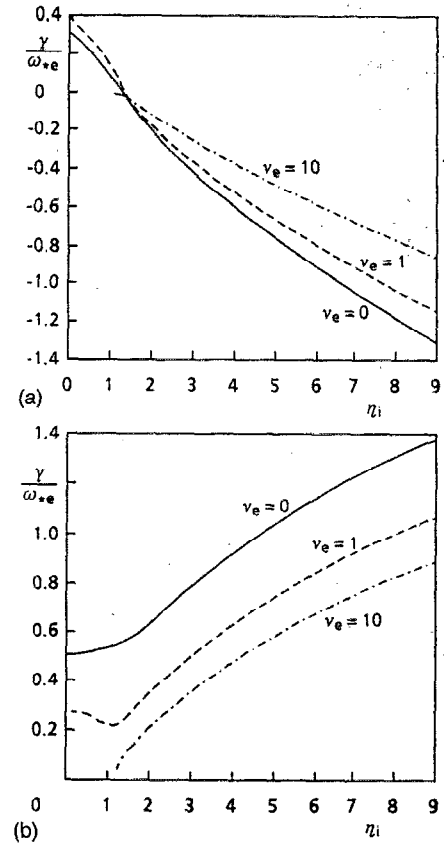

FIG. 5. Trapped-electron effects on the stability in the short-wavelength limit for $b_s=0.1$, $s=q=\tau=1$, $\epsilon_n=0.1$, and $\epsilon=0.15$. The frequencies (a) and the growth rates (b) of the mode versus η_i for different values of collisionality, $\nu_e=|\nu_{e\,\mathrm{eff}}/\omega_{*e}|$.

Ref. 23; while for finite q values, the effect of ion Landau damping tends to decrease the value of collisionality required for instability below $\eta_i=1.2$.

It is now important to check whether the various conditions used to derive Eq. (7) are in fact satisfied. The first condition concerns the strong coupling approximation. From the numerical analysis of Eq. (7), it is found that the eigenfunctions corresponding to modes close to marginal stability always have a moderate ballooning structure. As an example, Fig. 7 shows the eigenfunction obtained from Eq. (7) as a function of the variable z for $\epsilon_n=1$, $s=q=2$, $\tau=1$, and a nearly marginally stable mode. The half-width

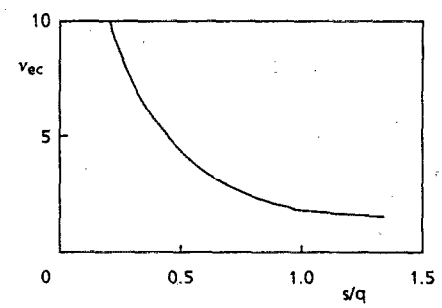

FIG. 6. The critical value $\nu_{ec}=|\nu_{e\,\mathrm{eff}}/\omega_{*e}|_c$ as a function of s/q for $b_s=0.1$, $\epsilon_n=0.1$, $\epsilon=0.15$, and $\tau=1$.

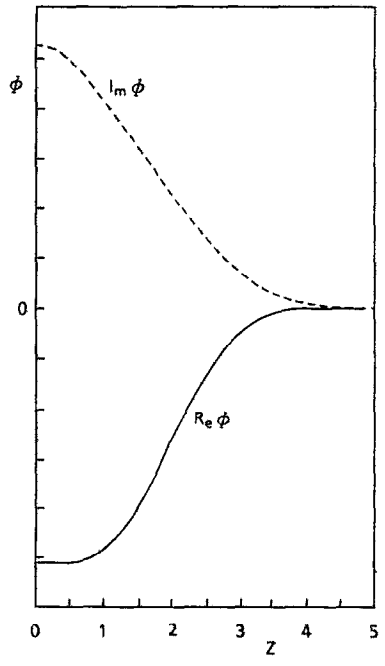

FIG. 7. The eigenfunction $\psi=\psi(z)$ near threshold for $s=q=2$, $\tau=1$, $b_s=0.1$, and $\epsilon_n=1.0$. The solid line represents the real part of ψ, the dashed line is the imaginary part.

of the eigenfunction is about $\Delta z\approx 2.0$. Within the strong coupling approximation, the width should be larger than the distance between mode rational surfaces, which corresponds to $\Delta z=1$. Therefore, the strong coupling approximation is satisfied *a posteriori*.

The second condition corresponds to neglecting trapped-ion effects. Note first that, within the present ordering, the perpendicular wavelength is shorter than the ion banana radius, since $k_\perp \rho_{bi}\approx k_\perp \rho_i \epsilon^{-1/2}\approx \epsilon_T^{1/4}\epsilon^{-1/2}$ $\approx 0.7\epsilon^{-1/2}>1$, for $\epsilon_T\approx\epsilon_{Tc}\approx 0.25$ and $\epsilon\approx 0.15$. Therefore, finite banana effects should make the trapped-ion response small in this parameter range. In addition, the ordering scheme implies that $\omega\approx\omega_{ti}\bar{\epsilon}_T^{1/4}>\omega_{bi}$, so an ion cannot see the trapping in the local magnetic mirror within a wave period. Nevertheless, trapped-ion corrections could play some role in the region of the parameter space where the mode frequency near threshold becomes very small. In the absence of trapped electrons this could indeed happen for low values of ϵ_n. However, when trapped electrons are considered, and for low or moderate values of collisionality, the mode is unstable also below the value $\eta_i\approx 1.2$ and the frequency always remains larger than ω_{bi}. In addition, in the flat density limit, the condition of $|\omega|\gg\omega_{bi}$ is always well satisfied, even without including the trapped-electron response.

Finally, the effects of ion–ion collisions are clearly irrelevant for this limit, since $\nu_{ii}/\omega\approx\nu_{ii}/\omega_{ti}\bar{\epsilon}_T^{1/4}\ll 1$ in the banana-plateau regime.

IV. LONG-WAVELENGTH TOROIDAL BRANCH

A general discussion of Eq. (10) can be found in Ref. 26, so, for the sake of completeness, we quote the main result only. As shown in Ref. 26, Eq. (10) yields the following threshold value:

$$\eta_i=1+\left[1+\frac{\epsilon_n^2}{q^2 b_s}\left(1+\frac{1}{\tau}\right)\right]^{1/2}. \tag{23}$$

Note that for long wavelengths this threshold is much higher than the short-wavelength threshold; therefore, the toroidal branch is more unstable at short wavelengths. As shown in Ref. 26, the same considerations can be applied to the low-shear regime.

It is interesting to note that Eq. (23) is very similar to the expression obtained by Dominguez and Rosenbluth[22] in the context of a local analysis in which the effect of parallel dynamics was retained by estimating $k_\parallel=1/qR$. The difference is a factor of $2^{1/2}$, which can be traced back to the assumption $k_\parallel\approx 1/qR$ made by Dominguez and Rosenbluth. This assumption should be replaced by $k_\parallel=1/(2qR)$, due to the variation of the eigenfunction on the connection length scale, such as $\cos(\theta/2)$.[25] In Fig. 1 the mode threshold is shown for $b_s=0.01$ (curve e). With decreasing b_s, curve c reduces to curve e.

V. LONG-WAVELENGTH SLABLIKE BRANCH

In order to solve the equation for the slablike branch, it is convenient to define an auxiliary ordering scheme. To this aim, we first note that the orbit correction term associated to the trapped-ion response in the collisionless regime is larger than the orbit correction term associated to the circulating ion response, since $k_\perp \rho_{bi}\approx k_\perp \rho_i\epsilon^{-1/2}\gg k_\perp \rho_i$. As a consequence, when such a term is balanced with the adiabatic electron response, the typical radial scale length tends to be of the order of ρ_{bi}, i.e., larger than the scale length of the sheared slab problem, which is of the order of the ion Larmor radius ρ_i. By assuming $k_\parallel v_{ti}/\omega\gg 1$, and balancing trapped-ion orbit corrections, adiabatic electron response, nonadiabatic trapped-ion response, and circulating ion response, the following optimal ordering is obtained:

$$k_\perp \rho_i\approx\epsilon_T\approx\epsilon^{1/2},\quad \omega\approx\omega_{*T}\frac{\epsilon_T^2}{\epsilon^{1/2}}\approx\epsilon_T\omega_{*T}\approx\omega_d. \tag{24}$$

Note that the above ordering is consistent with the long-wavelength ordering Eq. (11) for $\omega\ll\omega_{bi}$ or $k_\theta\rho_i\ll\epsilon_T^{1/2}/q$. On using the above ordering in Eq. (11), the following equation is obtained:

$$\frac{d^2\psi}{dz^2}-\frac{1}{b_s s^2 B_2^{(t)}}\left(1+\frac{1+\delta_T}{\tau}-A^{(t)}+i\pi^{1/2}\right.$$

$$\left.\times\frac{\omega-\omega_{*n}(1-\eta_i/2)}{z\omega_{ti}}\right)\psi=0. \tag{25}$$

In deriving Eq. (25), Eq. (12) has been approximated, as shown in Appendix B, by the following expression:

$$A^{(c)}=-\frac{1}{\beta_1}\left\{x^2\frac{\eta_i}{\tau\Omega}\left[1+xZ_i(x)\right]\right.$$
$$\left.+\left[1+\frac{1}{\tau\Omega}\left(1-\frac{\eta_i}{2}\right)\right]xZ_i(x)\right\}, \tag{26}$$

where

$$x=\left(\frac{b_s\tau}{2}\right)^{1/2}\frac{q\Omega}{\epsilon_{ne}z\beta_1},\quad \Omega=\frac{\omega}{\omega_{*e}}$$

and β_1,β_2 are constants defined in Appendix B.

Equation (25) is a Whittaker equation that can be solved in terms of confluent hypergeometric functions. By imposing the regularity condition in the origin and the condition of exponentially vanishing eigenfunction far from the mode rational surface, the following equation for the eigenvalue is obtained:

$$1+\frac{1+\delta_T}{\tau}-A^{(t)}+\frac{\pi}{4(1+n)^2}\frac{\tau[\omega-\omega_{*n}(1-\eta_i/2)]^2}{\omega_{ti}^2 b_s s^2 B_2^{(t)}}=0, \tag{27}$$

where n is a non-negative integer. In the collisionless regime, it is easy to find an explicit equation for the threshold for $n=0$:

$$1+\frac{1}{\tau}-\frac{(2\epsilon)^{1/2}}{\epsilon_T}=\frac{\pi}{16\ 2^{1/2}s^2}\left(\frac{2}{\eta_i}-1\right)\frac{q^2\epsilon^{1/2}}{1+2q^2\beta_3\epsilon_T}. \tag{28}$$

Neglecting the rhs, Eq. (28) yields, in the flat density regime,

$$\eta_{ic}=\left(1+\frac{1}{\tau}\right)(2\epsilon)^{-1/2}\epsilon_n. \tag{29}$$

This expression is very similar to that obtained in the short-wavelength regime when parallel dynamics is neglected.

The effect of ion collisionality becomes important for $\nu_{i\,\mathrm{eff}} > \omega \approx \omega_{Di}$. However, the ordering given by Eq. (24) continues to hold as long as the trapped-ion response is not significantly weakened in the orbit correction term, i.e., as long as $k_\perp \rho_{bi}(\omega/\nu_{i\,\mathrm{eff}}) > k_\perp \rho_i$ or $\nu_{i\,\mathrm{eff}} < \omega_{Di}\epsilon^{-1/2}$. For larger values of collisionality ($\nu_{i\,\mathrm{eff}} > \omega_{Di}\epsilon^{-1/2}$), the trapped-ion response can be neglected everywhere. In order to discuss such a limit, it is convenient to employ an approximation similar to the approximation used to derive Eq. (26), which, as shown in Appendix B, yields

$$B_1^{(c)}=-\frac{1}{\beta_1}\left\{x^2\frac{\eta_i}{\tau\Omega}\left[1+xZ_i(x)\right]\right.$$
$$\left.+\left[1+\frac{1}{\tau\Omega}\left(1+\frac{\eta_i}{2}\right)\right]xZ_i(x)\right\}, \tag{30}$$

$$B_2^{(c)}=B_1^{(c)}(1+2q^2\beta_2). \tag{31}$$

In this limit, Eq. (11) becomes equivalent to the slab equation solved by Hahm and Tang,[6] except for the factor $(1+2q^2\beta_2)$ in Eq. (31) which can be eliminated by rescaling the z variable. The final result is a straightforward generalization of Eq. (21):

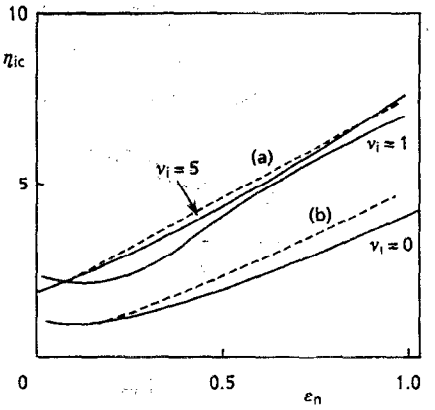

FIG. 8. Plot of η_{ic} vs ϵ_n for $b_s=0.01$, $s=q=\tau=1$, $\epsilon=0.15$, $\nu_{e\,\mathrm{eff}}=0$ and different values of the trapped-ion collisionality $\nu_i=|\nu_{i\,\mathrm{eff}}/\omega_{*e}|$ for the long-wavelength slablike branch. The dashed lines are the analytical result. Curve (a) is obtained from Eq. (32) and curve (b) is from Eq. (27).

$$\eta_{ic}=\eta_{i0}(b_s)+\alpha_s(b_s)\left(1+\frac{1}{\tau}\right)\frac{s}{q}(1+2q^2\beta_2)^{1/2}\epsilon_n\beta_1, \tag{32}$$

where η_{i0} and α_s are shown in Fig. 2 versus b_s. This result again shows that the long-wavelength limit is less unstable than the short-wavelength limit. The stabilizing effect is associated in this case with the finite radial excursion of circulating ions, which occurs on a time scale much shorter than the typical time scale of the mode and, on average, reduces the electrostatic field "seen" by the ions.

In Fig. 8 the threshold value η_{ic} is shown versus ϵ_n for different values of the effective collisionality of trapped ions. The nonadiabatic electron effects are neglected here because, for $|\nu_{i\,\mathrm{eff}}/\omega_{*e}| = O(1)$, the magnitude of the electron collisionality is large $[|\nu_{e\,\mathrm{eff}}/\omega_{*e}| \approx (m_i/m_e)^{1/2}]$, so the contribution from trapped electrons is negligible. With increasing ion collisionality, the curve obtained by solving Eq. (25) reduces to the threshold given by Eq. (32). The analytic results Eqs. (27) and (32) are also shown (dashed lines). It is apparent that the trapped ions play quite a significant destabilizing role.

For $|\nu_{i\,\mathrm{eff}}/\omega_{*e}| \approx (m_e/m_i)^{1/2}$, the trapped-electron effects should be taken into account. In Fig. 9 we plot the η_i mode threshold obtained by Eq. (11) versus ϵ_n for $\nu_{i\,\mathrm{eff}}=0$ and different values of $\nu_{e\,\mathrm{eff}}$. It is shown that trapped electrons provide only a small destabilizing effect in the flat density limit. In the peaked density limit, $\epsilon_n \ll 1$, trapped-electron effects become more important. In this limit, as shown in Ref. 23, the conventional electron branch also is unstable, corresponding to a mode that mainly propagates in the electron diamagnetic direction. However, ion Landau damping becomes more significant as the wavelength increases. Thus, the electron drift branch exists only for very low values of electron collisionality ($|\nu_{e\,\mathrm{eff}}/\omega_{*e}| < 1$) in the long-wavelength limit. For $\nu_{e\,\mathrm{eff}}=0$, the stability boundary corresponding to the electron branch is also shown in Fig. 9. Note the similarity to Fig. 3 of Ref. 23.

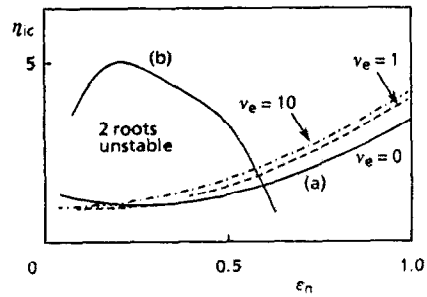

FIG. 9. Plot of η_{ic} vs ϵ_n for $\nu_{ii}=0$, $b_s=0.01$, $s=q=\tau=1$, $\epsilon=0.15$, and different values of the trapped-electron collisionality, $\nu_e = |\nu_{e\,\mathrm{eff}}/\omega_{*e}|$. Curves (a) and (b) correspond to the stability boundaries for ion and electron branches, respectively, for the collisionless case $\nu_e=0$.

It is important to stress that the effect of ion–ion collisions considered in this paper refers to situations typical of high-temperature tokamaks, i.e., characterized by values of the collisionality parameter $\nu_{*i} = \nu_{i\,\mathrm{eff}}/\omega_{bi}$ much smaller than one. For ν_{*i} values such that $\nu_{*i}\approx 1$ the effect of ion–ion collisions on both trapped and circulating ion response becomes important at long wavelengths and, as shown in Ref. 28, completely stabilizes the mode for $\nu_{ii}\approx\omega$, i.e., for $k_\theta\rho_i\approx\epsilon^{3/2}\nu_{*i}\epsilon_T$. For $\nu_{*i}\approx 10^{-1}$–10^{-2}, the last condition would correspond to $k_\theta\rho_i$ values that do not satisfy the condition for the validity of the ballooning representation. Therefore the long-wavelength slablike η_i threshold, for low collisionality, is determined by ion Landau damping.

The smallness assumption for the trapped-ion orbit correction term can be written as

$$\tfrac{1}{2}k_\theta^2\rho^2 s^2\theta_1^2\langle\alpha^2\rangle_t/\epsilon^2 \ll 1.$$

In order to check whether such a condition is indeed satisfied, we estimate θ_1^2 as $\theta_1^2=(d^2\phi/dz^2)/\phi$. The magnitude of the orbit correction is shown in Fig. 10 as a function of z. It is apparent that the value of the orbit correction term is always much smaller than unity.

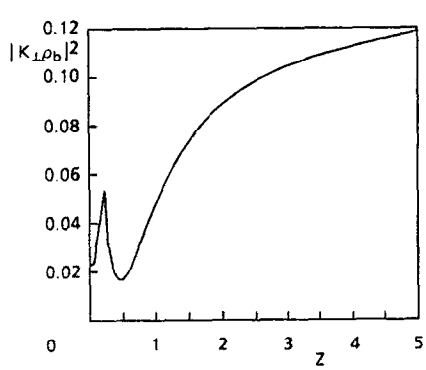

FIG. 10. Plot of the orbit correction term $0.5\,k_\theta^2\rho_i^2 s^2\theta_1^2\langle\alpha^2\rangle_t/\epsilon^2$ as a function of z for $b_s=0.01$, $s=q=\tau=1$, $\epsilon_n=1.0$, and $\eta_i=3.5$.

VI. CONCLUSIONS

In this paper, we have presented an analysis of the ion-temperature-gradient-driven mode in various parameter domains. In the short-wavelength ($k_\theta\rho_i\approx\epsilon_T^{1/4}$), moderate-shear limit, the effect of parallel dynamics has been discussed. A new expression of the linear threshold has been obtained:

$$\eta_{ic}=\begin{cases}1.2, & \epsilon_n=0,\\ \dfrac{4}{3}\left(1+\dfrac{1}{\tau}\right)\left(1+\alpha_T\dfrac{s}{q}\right)\epsilon_n, & \epsilon_n\geqslant\dfrac{1}{2}\left(1+\dfrac{1}{\tau}\right)^{-1},\end{cases}$$

with $\alpha_T\approx 2$. For low values of s/q ($s/q<0.3$), the parallel dynamics effect on the linear threshold is small, in agreement with the numerical findings of Ref. 19, where only the circulating ion response was retained, and not far from the estimate given in Refs. 12 and 28 where the full ion response was considered. In the limit $s/q\gg 1$, the sheared slab result of Ref. 6 can be recovered. When the effect of trapped electrons is considered, the threshold is modified only for low values of ϵ_n and η_i, i.e., for peaked density profiles. In particular, for low electron collisionality values, the mode remains unstable also below $\eta_i=1.2$, similar to the findings of Ref. 23, where the effect of parallel ion dynamics was neglected. However, at high collisionality, the destabilizing effect of trapped electrons is easily overcome by the stabilizing effect of Landau resonance, and the mode is stable in such a region of parameter space. Following the discussion of Ref. 23, the improvement in confinement by peaking the density profile can be easily achieved in high-density Ohmic discharges, while, at low collisionality, the analysis of the moderate shear limit predicts no significant improvement. Finally, the effect of trapped-ion dynamics has been shown to have little influence on the mode in this limit.

In the long-wavelength ($k_\theta\rho_i\ll\epsilon_T^{1/4}$) limit, the above-mentioned mode connects with the long-wavelength toroidal branch discussed in Refs. 25 and 26. The corresponding threshold value is given by Eq. (23):

$$\eta_i=1+\left[1+\frac{\epsilon_n^2}{q^2 b_s}\left(1+\frac{1}{\tau}\right)\right]^{1/2}.$$

In the same limit, a slablike branch also can be unstable. As the mode frequency is smaller than the bounce and transit frequency for $k_\theta\rho_i\ll\epsilon^{1/2}$, the stability of the modes belonging to this branch is strongly affected by the orbit corrections associated with the radial drifts of the ions. In particular, for sufficiently high ion–ion collisionality ($\nu_{i\,\mathrm{eff}} > \omega_{di}\epsilon^{-1/2}$, i.e., $\nu_{*i}=\nu_{i\,\mathrm{eff}}/\omega_{bi} > k_\theta\rho_i q/\epsilon$), the effect of trapped ions is negligible and the threshold is similar to the slab expression modified by the Pfirsch–Schlüter factor, Eq. (32):

$$\eta_{ic}=\eta_{i0}(b_s)+\alpha_s(b_s)\left(1+\frac{1}{\tau}\right)\frac{s}{q}(1+2q^2\beta_2)^{1/2}\epsilon_n\beta_1,$$

where η_{i0} and α_s are shown in Fig. 2 versus b_s. At low collisionality ($\nu_{i\,\mathrm{eff}} < \omega_{di}$, i.e., $\nu_{*i} < k_\theta\rho_i q/\epsilon^{-1/2} < 1$), the stability of the mode is dominated by the trapped-ion dy-

namics and the resulting threshold is given in the flat density limit by Eq. (29):

$$\eta_{ic}=\left(1+\frac{1}{\tau}\right)(2\epsilon)^{-1/2}\epsilon_n .$$

The resulting instability is basically a trapped-ion mode. With increasing ion collisionality, the threshold given by Eq. (29) reduces smoothly to the threshold given by Eq. (32). Trapped-electron effects do not play a significant role in this limit except at very low collisionality.

It is important to note that some features are common to all the above expressions of the threshold, such as the dependence on the ratio T_i/T_e which tends to yield a higher threshold value in the hot ion mode regime of operation, as experimentally observed in the Tokamak Fusion Test Reactor (TFTR) supershots.[38] On the contrary, there is no similarity for the dependence on the shear and on the safety factor, because the effect of parallel dynamics is not the same in all the considered limits. Moreover, it should also be stressed that the typical radial correlation length, estimated as the radial width of the eigenfunction, does not show the same scaling in the various regimes. To be specific, while at short wavelengths it scales as the toroidal ion Larmor radius, at long wavelengths, due to the effects of the radial drifts, it scales as the poloidal ion Larmor radius. This could provide the explicit current dependence of the energy confinement time observed in auxiliary heated experiments.

ACKNOWLEDGMENTS

One of the authors (SCG) wishes to acknowledge the support of the International Centre for Theoretical Physics (ICTP) Programme for Training and Research in Italian Laboratories.

APPENDIX A: DERIVATION OF THE QUASINEUTRALITY EQUATION FOR THE LONG-WAVELENGTH SLAB BRANCH

In order to derive the quasineutrality equation, we start from the gyrokinetic equation for ions:

$$\frac{v_\parallel}{qR}\,\partial_\theta H_i - i(\omega-\omega_{di})H_i = -i(\omega-\omega_{*Ti})J_0\frac{e\phi}{T_i}F_{Mi}, \tag{A1}$$

where

$$\omega_{di}=\omega_{db}+\omega_{d\psi},\quad \omega_{db}=\omega_{d0}\cos\theta,\quad \omega_{d\psi}=\omega_{d0}s\theta\sin\theta.$$

Since the mode structure is highly extended along the magnetic field line, it is possible to use a multiple scales analysis, where θ is separated as a fast variable $\theta_0\approx O(1)$ and a slow variable $\theta_1\approx O(\delta^{-1})$. Then $d/d\theta=\partial/\partial\theta_0+\delta\partial/\partial\theta_1$ and $H_i=H_0+\delta H_1$. At the lowest order, Eq. (A1) becomes

$$\omega_{ti}v_\parallel\,\partial_\theta H_0 + i\omega_{d\psi}H_0=0. \tag{A2}$$

The solution of Eq. (A2) is easily obtained:

$$H_0=\bar{H}_0(\theta_1)\exp\left(i\frac{\omega_{d0}s\theta_1}{\omega_{ti}\epsilon}\alpha\right), \tag{A3}$$

where

$$\alpha=\begin{cases}\dfrac{B_0}{B}v_\parallel, & \text{for trapped ions,}\\[2ex] \dfrac{B_0}{B}v_\parallel-\left\langle\dfrac{B_0}{B}v_\parallel\right\rangle_c, & \text{for circulating ions.}\end{cases}$$

In order to obtain Eq. (A3), the equality

$$\frac{\omega_{d\psi}}{v_\parallel}=-\frac{1}{\epsilon}\omega_{d0}s\theta_1 B_0\frac{\partial}{\partial\theta_0}\left(\frac{v_\parallel}{B}\right)$$

has been used. To solve the next order equation, we assume

$$H_1=\bar{H}_1(\theta_0,\theta_1)\exp\left(i\frac{\omega_{d0}s\theta_1}{\omega_{ti}\epsilon}\alpha\right). \tag{A4}$$

Then, at the first order, Eq. (A1) yields

$$\begin{aligned}\omega_{ti}v_\parallel\,\partial_{\theta 0}H_1 = &-i(\omega-\omega_{*T})J_0\phi F_M\exp\left(-i\frac{\omega_{d0}s\theta_1}{\omega_{ti}\epsilon}\alpha\right)\\ &+i(\omega-\omega_{db})H_0(\theta_1)\\ &-v_\parallel\,\omega_{ti}\left(\partial_{\theta 1}H_0(\theta_1)+i\frac{\omega_{d0}s}{\omega_{ti}\epsilon}\alpha H_0(\theta_1)\right).\end{aligned} \tag{A5}$$

For circulating ions, upon operating with the transit average on Eq. (A5), we obtain

$$\begin{aligned}&\omega_s\partial_{\theta_1}H_0(\theta_1)-i\left(\omega-\langle\omega_{db}\rangle_c-\frac{s}{\epsilon}\omega_{d0}\langle\alpha v_\parallel\rangle_c\right)H_0(\theta_1)\\ &\quad=-i(\omega-\omega_{*T})F_M J_0\phi_0\left(1-\frac{\omega_{d0}^2s^2\theta^2}{2\omega_{ti}^2\epsilon^2}\langle\alpha^2\rangle_c\right);\end{aligned} \tag{A6}$$

here

$$\langle\cdots\rangle_c\equiv\frac{(1/2\pi)\int_{-\pi}^{\pi}(d\theta_0/v_\parallel\,\omega_{ti})(\cdots)}{(1/2\pi)\int_{-\pi}^{\pi}(d\theta_0/v_\parallel\,\omega_{ti})},$$

and

$$\frac{1}{\omega_s}\equiv\frac{1}{2\pi}\int_{-\pi}^{\pi}\frac{d\theta_0}{v_\parallel\,\omega_{ti}},$$

$$\langle\alpha^2\rangle_c=\left\langle\frac{B_0^2}{B^2}v_\parallel^2\right\rangle_c-\left\langle\frac{B_0}{B}v_\parallel\right\rangle_c^2.$$

In the derivation of Eq. (A6), we expanded the exponential term in Eq. (A3) for small arguments, which corresponds to the assumption

$$\tfrac{1}{2}k_\theta^2\rho_i^2s^2\theta_1^2\langle\alpha^2\rangle c/\epsilon^2\ll 1.$$

For trapped ions, upon operating with the bounce average on Eq. (A5), we obtain

$$H_0(\theta_1)=\frac{(\omega-\omega_{*T})F_M J_0\phi_0}{\omega-\langle\omega_{db}\rangle_t-(s\omega_{d0}/\epsilon)\langle\alpha v_\parallel\rangle_t+i\nu_{i\,\mathrm{eff}}E^{-3/2}}\times\left(1-\frac{1}{2}k_\theta^2\rho_i^2q^2s^2\theta_1^2\frac{\langle\alpha^2\rangle_t}{\epsilon^2}\right);\tag{A7}$$

here

$$\langle\cdots\rangle_t\equiv\frac{(1/2\pi)\oint(d\theta_0/v_\parallel\,\omega_{ti})(\cdots)}{(1/2\pi)\oint(d\theta_0/v_\parallel\,\omega_{ti})}$$

and

$$\frac{1}{\omega_b}\equiv\frac{1}{2\pi}\oint\frac{d\theta_0}{v_\parallel\,\omega_{ti}}.$$

Again, we notice that the assumption

$$0.5k_\theta^2\rho_i^2s^2\theta_1^2\langle\alpha^2\rangle_t/\epsilon^2\ll1$$

has been made for the trapped-ion analysis.

Upon Fourier transforming Eq. (A6), and defining

$$H_0(z)=\int e^{-iz\theta_1}H_0(\theta_1)d\theta_1,$$

we have

$$H_0(z)=\frac{(\omega-\omega_{*T})F_M}{\omega-\langle\omega_{db}\rangle_c-z\omega_s}\int e^{-iz\theta_1}J_0\phi_0\times\left(1-\frac{1}{2}k_\theta^2\rho_i^2q^2s^2\theta_1^2\frac{\langle\alpha^2\rangle_c}{\epsilon^2}\right)d\theta_1\tag{A8}$$

for circulating ions. The nonadiabatic circulating ion responses can be written as

$$n_{ic}=\frac{1}{2\sqrt{\pi}}\sum_\sigma\int_c\frac{B\,d\mu\,dE}{|v_\parallel|}\bar{H}_0(\theta_1)\exp\left(i\frac{\omega_{d0}s\theta_1}{\omega_{ti}\epsilon}\alpha\right)J_0.\tag{A9}$$

Upon averaging over the fast variable θ_0 on Eq. (A9), it becomes

$$\bar{n}_{ic}(\theta_1)=\frac{1}{2\sqrt{\pi}}\omega_{ti}\int\frac{B\,d\mu\,dE}{\omega_s}H_0(\theta_1)\times\left(1-\frac{1}{2}k_\theta^2\rho_i^2q^2s^2\theta_1^2\frac{\langle\alpha^2\rangle_c}{\epsilon^2}\right)J_0.\tag{A10}$$

The corresponding Fourier conjugate quantity of $n_{ic}(\theta_1)$ is given by

$$\bar{n}_{ic}(z)=\frac{1}{2\sqrt{\pi}}\omega_{ti}\int\frac{B\,d\mu\,dE}{\omega_s}\left[\left(1-\frac{1}{2}k_\theta^2\rho_i^2\mu B_0\right)\frac{(\omega-\omega_{*T})F_M}{\omega-\langle\omega_{db}\rangle_c-z\omega_s}\phi(z)+\frac{(\omega-\omega_{*T})F_M}{\omega-\langle\omega_{db}\rangle_c-z\omega_s}\frac{1}{4}k_\theta^2\rho_i^2s^2\times\left(\mu B_0+2q^2\frac{\langle\alpha^2\rangle_c}{\epsilon^2}\right)\frac{\partial^2}{\partial z^2}\phi(z)+\frac{1}{4}k_\theta^2\rho_i^2s^2\left(\mu B_0+2q^2\frac{\langle\alpha^2\rangle_c}{\epsilon^2}\right)\frac{\partial^2}{\partial z^2}\left(\frac{(\omega-\omega_{*T})F_M}{\omega-\langle\omega_{db}\rangle_c-z\omega_s}\phi(z)\right)\right].\tag{A11}$$

In order to obtain the trapped-ion response, we follow a similar procedure by replacing the transit with the bounce response, yielding

$$\bar{n}_{it}(z)=\frac{1}{2\sqrt{\pi}}\omega_{ti}\int\frac{B\,d\mu\,dE}{\omega_b}\left[\left(1-\frac{1}{2}k_\theta^2\rho_i^2\mu B_0\right)\frac{(\omega-\omega_{*T})F_M\phi_0(z)}{\omega-\langle\omega_{db}\rangle_t-\frac{s}{\epsilon}\omega_{d0}\langle\alpha v_\parallel\rangle_t+i\nu_{i\,\mathrm{eff}}/E^{-3/2}}+\frac{(\omega-\omega_{*T})F_M\phi_0(z)}{\omega-\langle\omega_{db}\rangle_t-(s/\epsilon)\omega_{d0}\langle\alpha v_\parallel\rangle_t+i\nu_{i\,\mathrm{eff}}/E^{-3/2}}\frac{1}{4}k_\theta^2\rho_i^2s^2\left(\mu B_0+2q^2\frac{\langle\alpha^2\rangle_t}{\epsilon^2}\right)\frac{\partial^2}{\partial z^2}\phi(z)+\frac{1}{4}k_\theta^2\rho_i^2s^2\left(\mu B_0+2q^2\frac{\langle\alpha^2\rangle_t}{\epsilon^2}\right)\frac{\partial^2}{\partial z^2}\left(\frac{(\omega-\omega_{*T})F_M\phi_0(z)}{\omega-\langle\omega_{db}\rangle_t-(s/\epsilon)\omega_{d0}\langle\alpha v_\parallel\rangle_t+i\nu_{i\,\mathrm{eff}}/E^{-3/2}}\right)\right].\tag{A12}$$

The quasineutrality equation is then given by

$$\left(1+\frac{1}{\tau}(1+\delta_T)-A+\frac{b_s}{\tau}B_1\right)\phi_0-\frac{1}{2}\frac{b_s}{\tau}s^2\left(\frac{d^2}{dz^2}(B_2\phi_0)+B_2\frac{d^2}{dz^2}\phi_0\right)=0.\tag{A13}$$

After the transformation of $\phi=\psi/(B_2)^{1/2}$, the final eigenmode equation for the long-wavelength slab branch can be written as

$$\left(\frac{d^2}{dz^2}+Q(z)\right)\psi_0=0\tag{A14}$$

with

$$Q(z)=\frac{1}{4}\frac{[(d/dz)B_2]^2}{B_2^2}-\frac{1}{b_ss^2B_2}(1+\delta_T+\tau-A\tau)-\frac{B_1}{s^2B_2}.$$

APPENDIX B: A SIMPLE APPROXIMATION TO THE EXACT TWO-DIMENSIONAL INTEGRALS, EQS. (12)–(17)

In order to study the eigenmode equation for the long-wavelength slablike branch, it is possible to make a simple approximation to reduce the two-dimensional integrals, such as A, B_1, and B_2, to be one dimensional. For this purpose, we start with calculating the transit average and bounce average terms.

For circulating ions, we calculate the transit average terms by expanding in the small parameter ϵ', with $\epsilon'=2\epsilon/(1+\epsilon)$. It is found that

$$v_{\parallel}^{-1}=\frac{1}{\sqrt{E-\mu B}}=\frac{1}{\sqrt{E}\sqrt{\epsilon'/k^2}}\frac{1}{\sqrt{1-k^2\sin^2(\theta/2)}}\left(1-\frac{\epsilon'}{2}\sin^2\frac{\theta}{2}-\frac{(\epsilon')^2}{8}\sin^4\frac{\theta}{2}+\cdots\right). \tag{B1}$$

Here

$$\mu=\frac{v_{\perp}^2}{B},\quad k^2=\frac{2\epsilon}{1+\epsilon-(\mu B_0/E)}.$$

The circulating particle contribution corresponds to $\epsilon'<k^2<1$. By using the expression in Eq. (B1), the transit frequency ω_s is obtained:

$$\frac{\omega_s}{\omega_{tt}}=\frac{\pi}{2}\sqrt{\frac{\epsilon'}{k^2}}\sqrt{E}f(k^2); \tag{B2}$$

here

$$f(k^2)=\frac{1}{K}\left\{1+\frac{\epsilon'}{2}\frac{K_2}{K}+\frac{(\epsilon')^2}{8}\left[\frac{K_4}{K}+2\left(\frac{K_2}{K}\right)^2\right]\right\},$$

$$K_2=\frac{K-E_0}{k^2},$$

$$K_4=\frac{1}{k^2}\left[\frac{1}{3}\left(1+\frac{2}{k^2}\right)K-\frac{2}{3}\left(1+\frac{1}{k^2}\right)E_0\right],$$

where $K=K(k^2)$ and $E_0=E_0(k^2)$ are the complete elliptic integrals of the first and second kinds, and $\langle\alpha^2\rangle_c$, $\langle\omega_{db}\rangle_c$ are given by the following expression:

$$\langle\alpha^2\rangle_c=E\frac{\epsilon'}{k^2}F(\epsilon',k^2),$$

$$\langle\omega_{db}\rangle_c=\omega_{d0}f(k^2)\left(E\frac{\epsilon'}{k^2}(E_0-2E_2)+\frac{\mu B_0}{2}\frac{1}{1+\epsilon}(K-2K_2)\right), \tag{B3}$$

where

$$F(\epsilon',k^2)=\frac{E_0}{K}-\frac{\pi^2}{4}\frac{1}{K^2}+2\epsilon\frac{E_0}{K}+\frac{\epsilon'}{2}\frac{E_0}{K}\left(\frac{K_2}{K}-3\frac{E_2}{E_0}\right)-\epsilon'\frac{\pi^2}{4K^2}\frac{K_2}{K}+\epsilon^2\frac{E_0}{K}+\epsilon\epsilon'\frac{E_0}{K}\left(\frac{K_2}{K}-3\frac{E_2}{E_0}\right)+(\epsilon')^2\frac{E_0}{K}\left\{-\frac{3}{4}\frac{E_2}{E_0}\frac{K_2}{K}+\frac{3}{8}\frac{E_4}{E_0}+\frac{1}{8}\frac{K_4}{K}+\frac{1}{4}\left(\frac{K_2}{K}\right)^2-\frac{(\epsilon')^2}{4}\frac{\pi^2}{4}\frac{1}{k^2}\left[\frac{K_4}{K}+3\left(\frac{K_2}{K}\right)^2\right]\right\},$$

$$E_2=\frac{1}{3}\left[\left(2-\frac{1}{k^2}\right)E_0-\left(1-\frac{1}{k^2}\right)K\right],$$

$$E_4=\frac{1}{15}\left[\left(8-\frac{3}{k^2}-\frac{2}{k^4}\right)E_0-\left(4-\frac{2}{k^2}-\frac{2}{k^4}\right)K\right]. \tag{B4}$$

For trapped ions, we calculate the bounce-averaged terms by simply expanding in ϵ, and the bounce frequency ω_b is given by

$$\omega_b^{-1}=\frac{1}{\pi}\int_{-\theta_0}^{\theta_0}\frac{d\theta}{v_{\parallel}\omega_{ti}}=\frac{2}{\pi}\sqrt{\frac{2}{\mu B_0\epsilon}}K\left(\frac{1}{\gamma}\right)\frac{1}{\omega_{ti}}. \tag{B5}$$

The $\langle\alpha^2\rangle_t$, $\langle\alpha v_{\parallel}\rangle_t$ and $\langle\omega_{db}\rangle_t$ can be obtained:

$$\langle\alpha^2\rangle_t=2\mu B_0\epsilon\left[\left(\frac{1}{\gamma}\right)^2-1+\frac{E_0}{K}\right], \tag{B6}$$

$$\langle\alpha v_{\parallel}\rangle_t=E-\mu B_0(1+\epsilon)+2\mu B_0\epsilon\frac{E_0}{K}, \tag{B7}$$

$$\langle\omega_{db}\rangle_t=\frac{\omega_{d0}}{2}\left[\left(\frac{8}{3}E-\frac{2}{3}\mu B_0\right)\frac{E_0}{K}-\frac{4}{3}E_0+\frac{1}{3}\mu B_0(1+\epsilon)\right]; \tag{B8}$$

here

$$K=K\left(\frac{1}{\gamma}\right),\quad E_0=E_0\left(\frac{1}{\gamma}\right),\quad \frac{1}{\gamma}=\sqrt{\frac{E-\mu B_0-\mu B_0\epsilon}{2\mu B_0\epsilon}}=\sin\frac{\theta_0}{2}. \tag{B9}$$

In the lowest order, $E-\mu B_0\approx O(\epsilon)$, we have

$$\langle\omega_{db}\rangle_t+\frac{\omega_{d0}s}{\epsilon}\langle\alpha v_{\parallel}\rangle_t=\frac{\omega_{d0}}{2}E\left\{\left(2\frac{E_0}{K}-1\right)+4S\left[\left(\frac{1}{\gamma}\right)^2-1+\frac{E_0}{K}\right]\right\}\equiv\frac{\omega_{d0}}{2}EG\left(\frac{1}{\gamma}\right). \tag{B10}$$

To further simplify the integrals A, B_1, and B_2, we define

$$\beta_1=\frac{\pi}{2}f(k^2),$$

$$\beta_2=\frac{\langle\alpha^2\rangle_c}{\epsilon^2\mu B_0}=\frac{1}{\epsilon^2}\frac{\epsilon'/k^2}{1-\epsilon'/k^2}F(\epsilon',k^2),$$

$$\beta_3=\frac{\langle\alpha^2\rangle_t}{\epsilon^2\mu B_0}=\frac{2}{\epsilon}\left[\left(\frac{1}{\gamma}\right)^2-1+\frac{E_0}{K}\right],$$

$$\beta_4=\frac{\pi}{2}K\left(\frac{1}{\gamma}\right).$$

It can be shown by numerical calculation, performed for the case $\epsilon=0.15$, that both β_1 and β_2 depend very weakly on k^2 except in the very narrow region $k^2\approx 1$ for β_1 and $k^2\approx\epsilon'$ for β_2. Both β_3 and β_4 are also insensitive to $1/\gamma$. This fact allows us to simplify the integrals by taking β_1–β_4 to be constants. This approximation does not make any important quantitative change on the eigenvalue of the η_i mode. In this paper, we take $\beta_1=1$, $\beta_2=1.5$, $\beta_3=2.0$, and $\beta_4=1$. In addition, as shown in Ref. 36, the function $G(1/\gamma)$ can be taken as a constant value of 1.2 for finite shear ($s\approx 1$).

Upon making the above approximation, the two-dimensional integrals can be reduced to the following expressions:

$$A^{(c)}=\frac{1}{\beta_1 2\sqrt{\pi}}\sum_\sigma\int_c\frac{B_0\,d\mu\,dE}{\bar v_\parallel}\frac{(\omega-\omega_{*T})F_M}{\omega-z\bar v_\parallel\beta_1},\quad\text{(B11)}$$

$$B_1^{(c)}=\frac{1}{\beta_1 2\sqrt{\pi}}\sum_\sigma\int_c\frac{B_0\,d\mu\,dE}{\bar v_\parallel}\frac{(\omega-\omega_{*T})F_M}{\omega-z\bar v_\parallel\beta_1}\mu B_0,\quad\text{(B12)}$$

$$B_2^{(c)}=\frac{1}{\beta_1 2\sqrt{\pi}}\sum_\sigma\int_c\frac{B_0\,d\mu\,dE}{\bar v_\parallel}\frac{(\omega-\omega_{*T})F_M}{\omega-z\bar v_\parallel\beta_1}\times\mu B_0(1+2q^2\beta_2),\quad\text{(B13)}$$

for circulating ions. Here, the transit average of the magnetic drift frequency related to normal curvature, $\langle\omega_{db}\rangle_c$, has been neglected because it is a higher-order term $[O(\epsilon)]$. For trapped ions, we have

$$A^{(t)}=\frac{1}{2\sqrt{\pi}}\beta_4\sum_\sigma\int_t\frac{B_0\,d\mu\,dE}{\sqrt{\mu B_0\epsilon}}\times\frac{(\omega-\omega_{*T})F_M}{\omega-1.2\omega_{d0}E+i\nu_{i\,\mathrm{eff}}E^{-3/2}},\quad\text{(B14)}$$

$$B_1^{(t)}=\frac{1}{2\sqrt{\pi}}\beta_4\sum_\sigma\int_t\frac{B_0\,d\mu\,dE}{\sqrt{\mu B_0\epsilon}}\times\frac{(\omega-\omega_{*T})F_M}{\omega-1.2\omega_{d0}E+i\nu_{i\,\mathrm{eff}}E^{-3/2}}\mu B_0,\quad\text{(B15)}$$

$$B_2^{(t)}=\frac{1}{2\sqrt{\pi}}\beta_4\sum_\sigma\int_t\frac{B_0\,d\mu\,dE}{\sqrt{\mu B_0\epsilon}}\times\frac{(\omega-\omega_{*T})F_M}{\omega-1.2\omega_{d0}E+i\nu_{i\,\mathrm{eff}}E^{-3/2}}\mu B_0(1+2q^2\beta_3).\quad\text{(B16)}$$

Here,

$$\bar v_\parallel\equiv\sqrt{\frac{\epsilon'}{k^2}E}.$$

It is obvious that Eq. (B11) and Eq. (B12) can be readily simplified to the one-dimensional integrals, which can be written as follows:

$$A^{(c)}=-\frac{1}{\beta_1}\left\{x^2\frac{\eta_i}{\tau\Omega}[1+xZ_i(x)]+\left[1+\frac{1}{\tau\Omega}\left(1-\frac{\eta_i}{2}\right)\right]xZ_i(x)\right\},$$

$$B_1^{(c)}=-\frac{1}{\beta_1}\left\{x^2\frac{\eta_i}{\tau\Omega}[1+xZ_i(x)]+\left[1+\frac{1}{\tau\Omega}\left(1+\frac{\eta_i}{2}\right)\right]xZ_i(x)\right\},$$

$$B_2^{(c)}=B_1^{(c)}(1+2q^2\beta_2),$$

$$A^{(t)}=\frac{2}{\sqrt{\pi}}\beta_4\sqrt{2\epsilon}\int_0^\infty E^{1/2}\,dE\times\frac{1+(1/\tau\Omega)[1-\eta_i(E-\frac{3}{2})]e^{-E}}{1+1.2(\epsilon_{ne}/\tau\Omega)E+i(\nu_i/\Omega)E^{-3/2}},$$

$$B_1^{(t)}=\frac{2}{\sqrt{\pi}}\beta_4\sqrt{2\epsilon}\int_0^\infty E^{3/2}\,dE\times\frac{1+(1/\tau\Omega)[1-\eta_i(E-\frac{3}{2})]e^{-E}}{1+1.2(\epsilon_{ne}/\tau\Omega)E+i(\nu_i/\Omega)E^{-3/2}},$$

$$B_2^{(t)}=B_1^{(t)}(1+2q^2\beta_3).$$

Here,

$$\Omega=\frac{\omega}{\omega_{*e}},\quad x=\left(\frac{b_s\tau}{2}\right)^{1/2}\frac{q\Omega}{\epsilon_{ne}z\beta_1},\quad\epsilon_{ne}=\frac{L_{ne}}{R},\quad\nu_i=\frac{\nu_{i\,\mathrm{eff}}}{\omega_{*e}}$$

and Z_i is the plasma dispersion function for ions.

[1] F. Romanelli, Plasma Phys. Controlled Fusion **31**, 1535 (1989).
[2] L. I. Rudakov and R. Z. Sagdeev, Dokl. Akad. Nauk SSSR **138**, 581 (1961) [Sov. Phys. Dokl. **6**, 415 (1961)].
[3] B. Coppi, M. N. Rosenbluth, and R. Z. Sagdeev, Phys. Fluids **10**, 582 (1967).
[4] T. Antonsen, B. Coppi, and R. Englade, Nucl. Fusion **19**, 681 (1979).
[5] A. B. Hassam, T. M. Antonsen, Jr., J. F. Drake, and P. N. Guzdar, Phys. Fluids B **2**, 1822 (1990).
[6] T. S. Hahm and W. M. Tang, Phys. Fluids B **1**, 1185 (1989).
[7] B. Coppi and F. Pegoraro, Nucl. Fusion **17**, 969 (1977).
[8] W. Horton, D. I. Choi, and W. M. Tang, Phys. Fluids **24** 1077 (1981).
[9] G. Rewoldt, W. M. Tang, and E. A. Frieman, Phys. Fluids **21**, 1513 (1978).
[10] R. Marchand, W. M. Tang, and G. Rewoldt, Phys. Fluids **23**, 1164 (1980).
[11] G. Rewoldt and W. M. Tang, Phys. Fluids B **2**, 318 (1990).
[12] X. Garbet, L. Laurent, F. Morgues-Millot, J. P. Roubin, A. Samain, X. L. Zou, and J. Chinardet, in *Controlled Fusion and Plasma Physics*, Proceedings of the 18th European Conference, Berlin (European Physical Society, Geneva, 1991), Vol. 15C, Part IV, p. 21.
[13] S. C. Guo, L. Chen, S. T. Tsai, and P. N. Guzdar, Plasma Phys. Controlled Fusion **31**, 423 (1989)
[14] P. N. Guzdar, L. Chen, W. M. Tang, and P. H. Rutherford, Phys. Fluids **26**, 673 (1982)
[15] A. Jarmen, P Andersson, and J. Weiland, Nucl. Fusion **27**, 941 (1987).
[16] P. K. Shukla, Phys. Fluids B **2**, 848 (1990).
[17] R. R. Dominguez and R. E. Waltz, Phys. Fluids **31**, 347 (1988).
[18] P. Terry, W. Anderson, and W. Horton, Nucl. Fusion **22**, 487 (1982).

[19]F. Romanelli, Phys. Fluids B **1**, 1018 (1989).
[20]C. Z. Cheng and K. T. Tsang, Nucl. Fusion **21**, 643 (1981).
[21]S. C. Guo, Acta Phys. Sin. **31**, 17 (1982).
[22]R. R. Dominguez and M. N. Rosenbluth, Nucl. Fusion **29**, 844 (1989).
[23]F. Romanelli and S. Briguglio, Phys. Fluids B **2**, 754 (1990).
[24]W. M. Tang, G. Rewoldt, and L. Chen, Phys. Fluids **29**, 3715 (1986).
[25]L. Chen, S. Briguglio, and F. Romanelli, Phys. Fluids B **3**, 611 (1991).
[26]F. Romanelli, L. Chen, and S. Briguglio, Phys. Fluids B **3**, 2496 (1991).
[27]H. Biglari, P. H. Diamond, and M. N. Rosenbluth, Phys. Fluids B **1**, 109 (1989).
[28]X. Q. Xu and M. N. Rosenbluth, Phys. Fluids B **3**, 627 (1991).
[29]Y. K. Pu and S. Migliuolo, Phys. Fluids **28**, 1722 (1985); S. Migliuolo, Phys. Fluids **28**, 2778 (1985).
[30]O. Mathey and A. K. Sen, Phys. Fluids B **2**, 67 (1990).
[31]R. Paccagnella, F. Romanelli, and S. Briguglio, Nucl. Fusion **30**, 545 (1990).
[32]Y. B. Kim, P. H. Diamond, H. Biglari, and J. D. Callen, Phys. Fluids B **3**, 384 (1991).
[33]P. J. Catto, W. M. Tang, and D. E. Baldwin, Plasma Phys. **23**, 639 (1981).
[34]J. W. Connor, R. J. Hastie, and J. B. Taylor, Proc. R. Soc. London Ser. A **365**, 1 (1979).
[35]K. T. Tsang and P. J. Catto, Phys. Fluids **21**, 1381 (1978).
[36]J. C. Adam, W. M. Tang, and P. H. Rutherford, Phys. Fluids **19**, 56 (1976).
[37]J. B. Taylor, in *Plasma Physics and Controlled Nuclear Fusion Research, 1976* (International Atomic Energy Agency, Vienna, 1977), Vol. 2, p. 323.
[38]M. Zarnstorff, V. Arunasalam, C. W. Barnes, M. G. Bell, M. Bitter, H. S. Bosch, N. L. Bretz, R. Bundy, C. E. Bush, A. Cavallo, T. K. Chu, S. A. Cohen, P. L. Colestock, S. L. Davis, D. L. Dimock, H. F. Dylla, P. C. Efthimion, A. B. Erhardt, R. J. Fonck, E. D. Fredrickson, H. P. Furth, G. Gammel, R. J. Goldston, G. J. Greene, B. Grek, L. R. Grisham, G. W. Hammet, R. J. Hawryluk, H. W. Hendel, K. W. Hill, E. Hinnov, J. C. Hosea, R. B. Howell, H. Hsuan, R. A. Hulse, K. P. Jaehnig, A. C. Janos, D. L. Jassby, F. C. Jobes, D. W. Johnson, L. C. Johnson, R. Kaita, C. Kieras-Phillips, S. J. Kilpatrick, V. A. Krupin, P. H. LaMarche, B. LeBlanc, R. Little, A. I. Lysojvan, D. M. Manos, D. K. Mansfield, E. Mazzucato, R. T. McCann, M. P. McCarthy, D. C. McCune, K. M. McGuire, D. H. McNeill, D. M. Meade, S. S. Medley, D. R. Mikkelsen, R. W. Motley, D. Mueller, Y. Murakami, J. A. Murphy, E. B. Nieshmidt, D. K. Owens, H. K. Park, A. T. Ramsey, M. H. Redi, A. L. Roquemore, P. H. Rutherford, T. Saito, N. R. Sauthoff, G. Schilling, J. Schivell, G. L. Schmidt, S. D. Scott, J. C. Sinnis, J. E. Stevens, W. Stodiek, J. D. Strachan, B. C. Stratton, G. D. Tait, G. Taylor, J. R. Timbrlake, H. H. Towner, M. Ulrickson, S. Von Goeler, R. M. Wieland, M. D. Williams, J. R. Wilson, K. L. Wong, S. Yoshikawa, K. M. Young, and S. J. Zweben, in *Plasma Physics and Controlled Nuclear Fusion Research, 1988* (International Atomic Energy Agency, Vienna, 1989), Vol. 2, p. 191.